Regional differences of light absorption properties of fine particulate matter over the Tibetan Plateau: insights from HR-ToF-AMS and Aethalometer measurements

Xinghua Zhang[1,2,3], Jianzhong Xu[1*], Shichang Kang[1,3,7], Junying Sun[3,4], Jinsen Shi[5], Xinlei Ge[6], Chongshui Gong[2], Xuying Sun[2], Haolin Du[2]

[1]State Key Laboratory of Cryospheric Sciences, Northwest Institute of Eco-Environment and Resources, Chinese Academy of Sciences, Lanzhou 730000, China

[2]Key Laboratory of Arid Climatic Change and Reducing Disaster of Gansu Province, Key Laboratory of Arid Climatic Change and Disaster Reduction of CMA, Institute of Arid Meteorology, China Meteorological Administration, Lanzhou 730020, China

[3]University of Chinese Academy of Sciences, Beijing 100049, China

[4]Key Laboratory of Atmospheric Chemistry of CMA, Chinese Academy of Meteorological Sciences, Beijing 100081, China

[5]Key Laboratory for Semi-Arid Climate Change of the Ministry of Education, College of Atmospheric Sciences, Lanzhou University, Lanzhou 730000, China

[6]Jiangsu Key Laboratory of Atmospheric Environment Monitoring and Pollution Control, Collaborative Innovation Center of Atmospheric Environment and Equipment Technology, School of Environmental Science and Engineering, Nanjing University of Information Science and Technology, Nanjing 210044, China

[7]CAS Center for Excellence in Tibetan Plateau Earth Sciences, Beijing 100085, China

Corresponding author: Jianzhong Xu (jzxu@lzb.ac.cn)

Key Points:

- Aerosol chemical and light absorption properties were studied in the Tibetan Plateau (TP) by using a series of online measurements.
- Brown carbon contributed significantly to the light absorption in the southern TP and mainly attributed to the biomass burning sources.
- Distinct light absorption and radiative forcing in the TP suggesting their regional difference on aerosol sources and optical properties.

Abstract

Tibetan Plateau (TP) has aroused widely scientific concerns in recent decades owning to its important effects on regional climatic and cryospheric changes, hydrological cycle, and environments. However, our understandings on the chemical and optical properties of aerosols are still limited at those regions. In this study, regional difference of aerosol light absorption properties were explored at three remote TP sites, including Qomolangma Station (QOMS) in the southern TP, Nam Co Station (NamCo) in the central TP, and Waliguan Observatory in the northeastern TP. Although aerosol mass concentration at QOMS was less than half of that at Waliguan, the light absorption coefficient at QOMS was nearly 5 time higher than that at Waliguan, mainly as a result of the high contributions of light-absorbing carbonaceous aerosols in the southern TP from the long-range transported biomass burning emissions of South Asia. An improved method was used to derive the near-realistic absorption Ångström exponent for pure black carbon (BC) particles. BC dominated the light absorption at all wavelengths, whereas brown carbon (BrC) contributed more than 30% of the light absorption at 370 nm at QOMS and ~ 20% at Waliguan and NamCo. The major contributor to BrC light absorption at QOMS was the biomass burning related organic aerosol. Radiative transfer simulations also showed the highest atmospheric radiative forcings at QOMS among the three campaigns. The significant regional differences of aerosol light absorption properties in the TP might be related tightly with the different aerosol sources and chemical processes.

Plain Language Summary

Brown carbon is a group of organic compounds that preferentially absorbs solar light at short wavelengths and has aroused widely scientific concerns, however, understanding on the physicochemical properties is still limited, especially at remote regions. Combining two online instruments and adopting a novel approach, our study focuses on the absorption properties and aerosol radiative forcing of brown carbon in the Tibetan Plateau, and evaluate the regional differences on aerosol physicochemical properties, which should be taken into account carefully in the future climate model for evaluation of radiant energy budget and potential impacts on climatic and cryospheric changes over the Third Pole environments.

1 Introduction

Light-absorbing carbonaceous aerosols, accounting for a large fraction of atmospheric aerosols, have profound impacts on the Earth's climate systems (Bond et al., 2013; Laskin et al., 2015). Black carbon (BC) is one of the well-known component of light-absorbing carbonaceous aerosol in the atmosphere and also be the second global warming agent only after carbon dioxide when estimating its total direct radiative forcing from all BC sources up to +1.48 W m^{-2} (Bond et al., 2013). In addition to BC, a group of organic compounds that known as brown carbon (BrC) for its light brownish color, also absorb the solar radiation significantly, especially at the short visible to ultraviolet wavelengths (Andreae & Gelencsér, 2006; Laskin et al., 2015). A global climate model has simulated that BrC could contribute 19% of the total absorption by anthropogenic aerosols, while as high as 72% of the absorption was attributed to BC (Feng et al., 2013), however, the contribution of BrC could also make up to more than 50% over regions influenced significantly by biomass burnings (Favez et al., 2009; Feng et al., 2013). Accurate simulation of the radiative forcing of light-absorbing carbonaceous aerosols is quite crucial to evaluate the global climate change and warming effects. However, it also highlights the need for

the understanding of sources, formation processes, chemistry, mixing states, and absorption properties of those light-absorbing aerosols.

The incomplete combustions from biomass burning have been recognized as the main primary source for both BC and BrC in previous studies (Laskin et al., 2015; Lin et al., 2016; Washenfelder et al., 2015). Recently, the emission of coal combustion is also found containing significant amounts of BrC (Yan et al., 2017). Some high molecular weight light-absorbing compounds, especially those highly unsaturated nitrogen-containing compounds from multiphase secondary formation processes including gas-phase photooxidation, aqueous reactions and in-cloud processing, can also attributed to BrC and generally categorized as the secondary BrC (Chen et al., 2018b; Laskin et al., 2015; Lin et al., 2016; Lu et al., 2019; Sun et al., 2007; Ye et al., 2019). Those diverse sources and complex chemical transformation processes make it quite challenging to understand the chemical structures, optical properties as well as radiative forcing effects of BrC. Besides the difference of chemical properties between BC and BrC, there is also difference on physical properties between them, e.g., the wavelength dependent property, which is generally described using the parameter of absorption Ångström exponent (AAE). Previous studies have revealed that BC absorbed the solar radiation over a broad spectrum from ultraviolet into infrared wavelengths yet with a weak dependence on wavelength, i.e., low AAE value around one, whereas the light absorption of BrC increased sharply from the short visible to ultraviolet wavelengths and hence was characteristic of higher AAE values (Corr et al., 2012; Lack & Langridge, 2013; Laskin et al., 2015; Moosmüller et al., 2011). This difference of wavelength dependency between BC and BrC and the assumed uniform AAE value for BC (AAE_{BC}) have been widely used in previous studies to calculate the light absorption attributed to BrC, which could not be measured directly like the absorption coefficient of BC using online instruments due to the diverse sources and complex chemical compositions (Lack & Langridge, 2013). However, the light absorption of BC may enhance significantly after coating with other non-BC materials, which was often referred to as lensing effect (Jacobson, 2001). Previous studies have found an obvious shift of AAE_{BC} value up to ~ 1.7 due to the lensing effect, depending strongly on the optical properties and sizes of the core and coating materials, mixing states, as well as morphologies (Lack & Cappa, 2010; Li et al., 2019). Therefore, quantifying the near realistic AAE_{BC} value accurately is essential for the apportionment of light absorption to different light-absorbing aerosols.

Tibetan Plateau (TP), often called as the "third pole", is the highest and largest highland in the world (Yao et al., 2012). Moreover, the TP is also called as the "hot spot" or "sensitive area" for global climate change due to its significant impacts on regional and global climate (Duan & Wu, 2005; Kang et al., 2010), and its dramatic and significant climate warming (Qin et al., 2009; Wang et al., 2008; Xu et al., 2009). Besides the greenhouse gases that considered as the key factor to climate warming, abundant carbonaceous aerosols, particularly the light-absorbing carbonaceous aerosols have attracted global attentions in recent years due to their important roles in the TP warming (Cao et al., 2011; Kang et al., 2019; Ramanathan & Carmichael, 2008). The insightful investigations on the sources, chemical compositions and light absorption properties of carbonaceous aerosols, especially for the highly complex BrC on the TP are needed. To date, numerous studies have reported the absorption properties of BrC on the TP, however, most of them focused on the extracted water-soluble BrC or methanol-soluble BrC from off-line filter measurement with relatively low time resolutions (Kirillova et al., 2016; Li et al., 2016b; Wu et al., 2020; Xu et al., 2020; Zhang et al., 2017; Zhu et al., 2018). Only few real-time measurements of the particle light absorption using online optical instruments were

conducted in recent years, but mostly at the southern TP locations (Chen et al., 2018a; Wang et al., 2019a; Zhao et al., 2019; Zhu et al., 2017). Understanding of the particle light absorption property as well as its relationships with sources and chemistry on the TP is still limited until now.

In this study, the real-time light absorption properties of BC and BrC from three high-altitude remote sites located in the southern, central, and northeastern TP, respectively, were studied based on the online Aethalometer measurements. An improved AAE method was used to derive the near realistic AAE value for pure BC particle and then obtained the BrC light absorption coefficients indirectly. Furthermore, the light absorptions of BrC were attributed to different sources obtained by co-located measurement of a high-resolution time-of-flight mass spectrometer in each study. The purpose of this study is to elucidate the regional difference on chemical and optical properties of aerosols over the TP.

2 Methodology

2.1 Sampling sites

During 2015–2017, three field studies were conducted by our team at three high-altitude background observatories in the TP, i.e., the Nam Co Station (NamCo; 90°57′ E, 30°46′ N; 4730 m a.s.l.) between 31 May and 1 July 2015, the Qomolangma Station (QOMS; 86°57′ E, 28°22′ N; 4276 m a.s.l.) between 12 April and 12 May 2016, and the Waliguan Baseline Observatory (Waliguan; 100°54′ E, 36°17′ N; 3816 m a.s.l.) during 1–31 July 2017, respectively. The QOMS locates on the northern toe of the Mt. Everest at the south edge of the TP, while the NamCo locates near the Nam Co Lake at the central TP and the Waliguan locates at the mountaintop of the Mt. Waliguan at the northeast edge of the TP, as shown in Figure 1. All three high-altitude stations were isolated from residential areas with relatively limited local anthropogenic aerosol source emissions. Detailed descriptions for each study can be found in our previous publications (Wang et al., 2017; Xu et al., 2018; Zhang et al., 2018; Zhang et al., 2019).

2.2 Instrumentation

A suite of online instruments were deployed to measure the particle physicochemical and optical properties during each field study. Specifically, a seven wavelengths (370, 470, 520, 590, 660, 880, and 950 nm) Aethalometer (model AE33, Magee Scientific Corp., Berkeley, CA, USA) was used to measure the aerosol light absorption and BC mass concentration at a time resolution of 5 minutes during the QOMS campaign, meanwhile a parallel photoacoustic extinctiometer (PAX, Droplet Measurement Technologies Inc., Boulder, CO, USA) also measured the particle light absorption and scattering coefficients at 405 nm and BC mass concentration at 5 min time resolution. Similarly, a seven wavelengths AE31 Aethalometer and a PAX were deployed at a time resolution of 1 hour during the Waliguan campaign. A seven wavelengths AE31 Aethalometer and a multi-angle absorption photometer (MAAP, model 5012, Thermo Electron Corp., MA, USA) for BC mass concentrations and aerosol light absorption properties at 670 nm were conducted at 5 min time resolution during the NamCo campaign. In all three studies, a high-resolution time-of-flight aerosol mass spectrometer (HR-ToF-AMS, Aerodyne Research Inc., Billerica, MA, USA) was deployed for the measurements of size-resolved chemical compositions (organics, sulfate, nitrate, ammonium, and chloride) of non-refractory submicron particulate matter (NR-PM_1). All instruments above were arranged in an

air-conditioned room or trailer where air temperature was controlled at ~20 °C. Ambient particles were generally sampled through similar inlet systems during the three campaigns, including a $PM_{2.5}$ cyclone (model URG-2000-30EH, URG Corp., Chapel Hill, NC, USA) for removing coarse particles and a Nafion dryer to dry the ambient air stream before entering into the instruments. Details of the instrument operations and setups as well as the data processing of HR-ToF-AMS datasets have been described elsewhere (Xu et al., 2018; Zhang et al., 2018; Zhang et al., 2019). Note that all the date and time used in this study are reported in Beijing Time (BJT: UTC +8 h).

2.3 Data treatment of light absorption datasets

2.3.1 Correction on Aethalometer data

The working principle of an Aethalometer is to collect the aerosol particles on the filter and measure the light attenuation through a particle-laden sample spot and a particle-free reference part of the filter. Two correction parameters (k and C), which are used to describe the nonlinear filter-based loading effects and the filter multiple scattering effects, respectively, were introduced to convert the particle light attenuation coefficients at the filter substrate to the light absorption coefficients (B_{abs}) of particles suspended in the air (Collaud Coen et al., 2010; Weingartner et al., 2003).

As a new Aethalometer model used during the QOMS campaign, the AE-33 adopts a compensation algorithm based on the dual-spot measurements to obtain the real-time loading compensation parameter k and automatically corrects the filter-based loading effects (Drinovec et al., 2015). Whereas the datasets from the Aethalometer AE31 during the Waliguan and NamCo campaigns are needed to be compensated manually for the filter-based loading effects using the Weingartner method (Weingartner et al., 2003). Specifically, a customized Aethalometer data processing tool (Wu et al., 2018) was used to correct the AE31 data for loading effects during the two campaigns in this study. A default C value of 1.57 was widely recommended to compensate the scattering effects caused by tetrafluoroethylene (TFE)-coated glass filter in previously studies (Drinovec et al., 2015). However, some studies suggested that C value was not a constant and might be site-specific (Collaud Coen et al., 2010). In this study, the PAX absorption data at 405 nm was used to derive the site-specific C values during the QOMS and Waliguan campaigns. The comparisons of particle B_{abs} at 405 nm that measured from PAX and calculated from Aethalometers according to the measured B_{abs} at 370 nm and the fitted AAE during the QOMS and Waliguan campaigns were displayed in Figures S1-S2, respectively. Tight correlations (R^2 = 0.94 and 0.79) were found between them during the two campaigns and the Aethalometer absorption coefficients were both higher than the PAX absorption coefficients, with slopes of 2.23 and 2.28, respectively. Therefore, final C values of 3.5 (= 2.23×1.57) and 3.6 (= 2.28×1.57) were set for correcting the filter scattering effects of the Aethalometer data during the QOMS and Waliguan campaigns, respectively. These values were comparable with those from other Aethalometer measurements in previous studies (Collaud Coen et al., 2010; Li et al., 2019; Qin et al., 2018; Wang et al., 2019b). For the NamCo campaign, we used the measured BC mass concentrations from MAAP at 670 nm to correct the BC mass concentrations and B_{abs} from AE31 due to the absence of PAX measurement (Figure S3). Note that the PAX and MAAP instruments, which were used for the above corrections of Aethalometer data, were all calibrated before start of each campaign, e.g., using ammonium sulfate particles and black smoke from kerosene lamp to calibrate the light scattering and absorption for the PAX, respectively.

2.3.2 Calculations of AAE and BrC light absorption

The default mass absorption cross-section (MAC), used for the conversion of measured Aethalometer data between light absorption coefficients and BC mass concentrations, were 18.47, 14.54, 13.14, 11.58, 10.35, 7.77, and 7.19 $m^2\ g^{-1}$ for the seven wavelengths, respectively. The AAE value can be calculated through a power-law fitting of the absorption coefficients among all the wavelengths following the Beer–Lambert's law. An AAE value of unity has been generally recommended for the pure BC aerosol, however, the higher AAE values than unity were found for most of the ambient studies, indicating important contributions from BrC to the particle light absorption. In order to quantitatively analyze the BrC contributions to the total particle light absorption, the BrC light absorption at a short wavelength λ_1 (B_{abs,BrC,λ_1}) can be calculated from the traditional AAE method (Lack & Langridge, 2013), as described in the following equations (1) and (2):

$$B_{abs,BrC,\lambda_1} = B_{abs,\lambda_1} - B_{abs,BC,\lambda_1} \quad (1)$$

$$B_{abs,BC,\lambda_1} = B_{abs,BC,\lambda_2} \times (\lambda_2 / \lambda_1)^{AAE_{BC}} \quad (2)$$

where B_{abs,λ_1} and B_{abs,BC,λ_1} are the total and BC particle light absorption coefficients at the short wavelength λ_1 between 370 nm and 660 nm, while B_{abs,BC,λ_2} are the BC particle light absorption coefficients at a longer wavelength λ_2 of 880 nm, at which BrC is assumed to have negligible contribution to particle light absorption. AAE_{BC} was the AAE caused by the pure BC particle and commonly used as unity in previous study. However, most recent studies have revealed the important lensing effects caused by the non-BC matters coating on the pure BC cores (Corr et al., 2012; Gyawali et al., 2009; Lack & Langridge, 2013; Lewis et al., 2008), which enhanced the real AAE values more significantly and lead to +7% to −22% uncertainty for the attributed BC light absorption (Lack & Langridge, 2013). In this study, an improved AAE method adopted from Yuan et al. (2016) were used to calculate the realistic AAE_{BC} values during the three campaigns. The details of this method are described in Section 3.3.1.

2.3.3 Estimation of direct radiative forcing

The aerosol direct radiative forcing (DRF) was modelled by the widely used Santa Barbara DISORT (Discrete Ordinate Radiative Transfer) Atmospheric Radiative Transfer (SBDART) model in the shortwave spectral range of 0.25−4.0 μm. SBDART was a software tool computed the plane-parallel radiative transfer under both clear and cloudy conditions (Ricchiazzi et al., 1998). Aerosol parameters including the aerosol optical depth (AOD), single scattering albedo (SSA), Ångström exponent (AE) and asymmetric (ASY) were the four crucial input parameters in the estimation of aerosol DRF in SBDART model, which could be estimated using the measured mass concentrations of organic carbon (OC), BC, and water soluble ions (WSIs) from corresponding filter samplings in the Optical Properties of Aerosol and Cloud (OPAC) model (Hess et al., 1998) during the three campaign, respectively. In brief, the net fluxes (difference between the downward and upward radiation fluxes) with and without the investigated variable were calculated twice times in this model under cloud-free conditions at both the earth's surface (SUR) and the top of the atmosphere (TOA). The differences of net fluxes between the two simulations were then considered as the DFRs of the specific investigated variable at the SUR and TOA, respectively. Finally, the DRF in the atmosphere (ATM) was obtained using the DRF at TOA subtracts DRF at SUR in this study. The details of the model description can be found in previous studies (Gong et al., 2017; Xin et al., 2016).

3 Results and discussions

3.1 Overview of PM_1 chemical characteristics at three sites

Figure 1 shows the campaign-averaged chemical compositions of submicron particulate matter (PM_1 = NR-PM_1 + BC) measured by the HR-ToF-AMS and PAX/MAAP at the three campaigns. Relatively lower PM_1 mass concentrations (2.0 and 4.4 μg m^{-3}) were observed at NamCo and QOMS, compared with that at Waliguan (9.1 μg m^{-3}). Moreover, distinctly different chemical compositions were also found at the three sites. Secondary inorganic species (sulfate, nitrate and ammonium) contributed more than 60% of total PM_1 during the Waliguan campaign whereas just 24% and 20% during the NamCo and QOMS campaigns, respectively. Organics and BC contributed 54.4% and 25.0% of PM_1, respectively, at QOMS while organics contributed as high as 68% of PM_1 at NamCo. Considering the minor local aerosol sources over the TP due to the sparse population and few anthropogenic activities, this difference on aerosol chemical speciation may mainly be attributed to the differences in aerosol sources in the regions around them. Aerosols at the south edge of TP mainly related to the long-range transport of biomass burning emissions from South Asia (Cong et al., 2015a; Cong et al., 2015b; Li et al., 2016a; Lüthi et al., 2015; Zhang et al., 2018), whereas air masses to Waliguan were mainly from the inland of the northwestern China with short transport distance (Zhang et al., 2019). Anthropogenic aerosol emissions from coal combustion and/or other fossil fuel usage could easily be transported to the northeast edge of TP via the mountain-valley breeze during the summer season (Li et al., 2015; Xu et al., 2014; Zhang et al., 2014). Although the dominant air masses during the NamCo campaign also originated from the South Asia, much longer transport distance and half of the sampling period during monsoon season led to the lowest PM_1 mass concentration among the three campaigns and with more oxidized organic aerosols dominated (Xu et al., 2018).

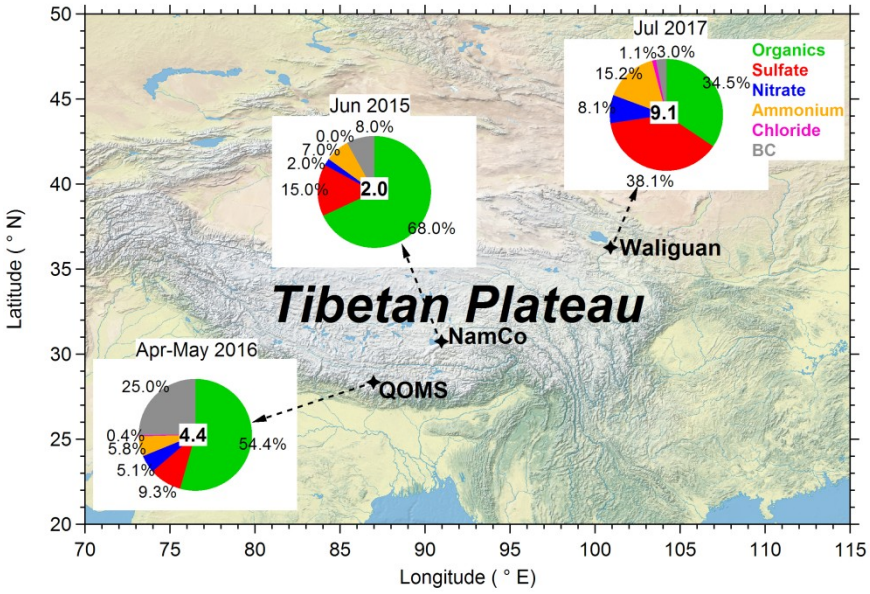

Figure 1. Locations of the sampling sites, i.e., Qomolangma station (QOMS), Nam Co station (NamCo) and Waliguan Baseline Observatory (Waliguan), across the Tibetan Plateau. The map is plotted in Igor Pro (Wavemetrics Inc.) using IgorGIS data downloaded from http://www.wavemetrics.net/Downloads/IgorGIS/ (last access: 22 Jul 2020). The inserted piecharts are the average chemical compositions of submicron

particulate matter (PM_1) during each sampling period, while the values in the center represent the average PM_1 mass concentrations with units of μg m^{-3}.

3.2 Comparisons of aerosol light absorption properties at the three sites

Box-plots of the particle light absorption coefficients (B_{abs}) at the seven wavelengths measured by Aethalometers during the three campaigns are showed in Figure 2. The B_{abs} decreased significantly with the increasing wavelength during all campaigns, following the inherent wavelength dependency property. The average B_{abs} at 370 nm ($B_{abs,370}$) were 13.4, 2.7, and 3.3 Mm^{-1} at QOMS, Waliguan and NamCo, respectively. Although relatively lower aerosol mass loading was found at QOMS than that at Waliguan (4.4 vs. 9.1 μg m^{-3}), the $B_{abs,370}$ at QOMS was nearly 5 time higher than Waliguan, mainly due to the important contributions of light-absorbing matters, e.g., BC, from biomass burning emissions at the south edge of TP (Zhang et al., 2018). In addition, Xu et al. (2020) also found distinct higher light absorption efficient of BrC at QOMS than that of Waliguan through water extraction of filter samples collected during these two studies. The $B_{abs,370}$ at QOMS was comparable with that (15.0 Mm^{-1}) measured at Lulang (Zhu et al., 2017), another remote site located at the southeastern TP which is also influenced significantly by the biomass burnings from South Asia. However, this value was much lower than those (35.8−231.3 Mm^{-1}, Table 1) measured at urban sites in China (Li et al., 2019; Qin et al., 2018; Wang et al., 2018; Xie et al., 2019; Zhu et al., 2017), reflecting the overall background nature of the remote sites over the TP. Diurnal variations of the B_{abs} at each wavelength during each campaign (Figure S4) are quite consistent with those of PM_1 chemical species (Xu et al., 2018; Zhang et al., 2018; Zhang et al., 2019). The distinct decrease of B_{abs} at QOMS in the afternoon was related to the enhanced wind speed and boundary layer height in the valley, while the increases of B_{abs} in the afternoon during Waliguan and NamCo campaigns might be related with the favorable transport mechanism of aerosol plume (Xu et al., 2018; Zhang et al., 2018; Zhang et al., 2019). The AAE values are fitted with campaign-averaged values to be 1.73, 1.12 and 1.28 at QOMS, Waliguan and NamCo, respectively. The higher AAE at QOMS suggested its higher contribution of BrC. Besides, non-BC materials coated on BC cores causing the lensing effect may also lead to a shift of the AAE (Li et al., 2019). The AAE values during the entire sampling periods of the three campaigns were in the range of 1−3 for QOMS and 0.6−2.4 for NamCo, whereas shift to lower values of 0.6−2.0 at Waliguan (Figure 2).

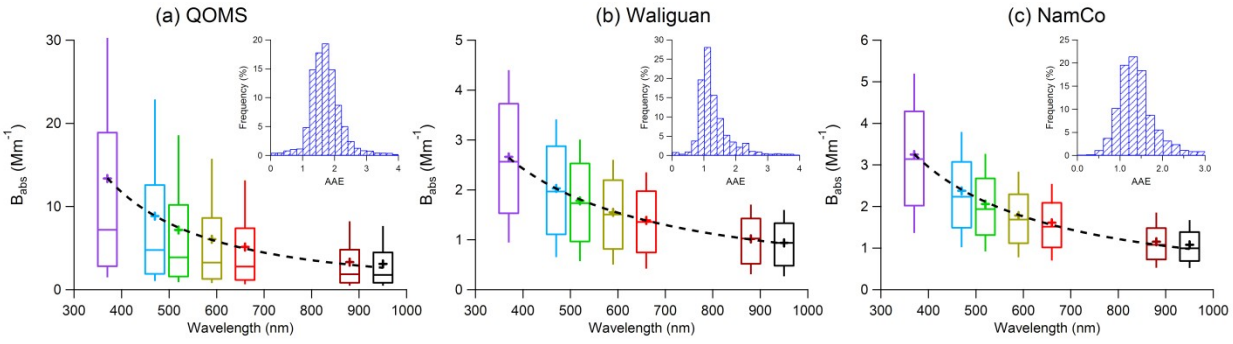

Figure 2. Box-plots of the light absorption coefficients (B_{abs}) at seven wavelengths (from 370 nm to 950 nm) measured by Aethalometers at the three sampling sites. The dashed lines show the power-law fit of the average B_{abs} for the calculation of absorption Ångström exponent (AAE). The inserted plots are the histograms of AAE values over each measurement campaign.

Table 1. A summary of the campaign-average values of total particle light absorption coefficient ($B_{abs,370}$), BrC light absorption coefficient ($B_{abs,BrC,370}$) and its contribution ($fB_{abs,BrC,370}$) at 370 nm, and the calculated absorption Ångström exponents for total particle, BC and BrC (AAE, AAE_{BC} and AAE_{BrC}) in this study and those in other studies conducted at the remote TP sites and urban sites in China.

Site	Period	$B_{abs,370}$ (Mm^{-1})	$B_{abs,BrC,370}$ (Mm^{-1})	$fB_{abs,BrC,370}$ (%)	AAE	AAE_{BC}	AAE_{BrC}	References
QOMS	Apr-May	13.4	4.4	33.1	1.73	1.187	4.21	This study
Waliguan	Jul	2.7	0.6	22.4	1.12	1.042	3.11	This study
NamCo	Jun	3.3	0.7	21.3	1.28	1.086	3.71	This study
Lhasa	Sep	53.0	4.2	8.0	1.04	1	3.30	Zhu et al. (2017)
Lulang	Sep-Nov	15.0	4.8	32.0	1.18	1	3.80	Zhu et al. (2017)
Panyu	Nov-Dec	56.0	13.2	23.6	1.43	Corr.[a]		Qin et al. (2018)
Nanjing	Annual	35.8	6.3	16.7	1.20	Corr.		Wang et al. (2018)
Guangzhou	Nov-Jan	68.9	23.5	34.1		Corr.		Li et al. (2019)
Beijing	Nov-Dec	231.3	106.4	46.0	1.58	1		Xie et al. (2019)

[a]The AAE_{BC} value that used for the calculation of BrC light absorption coefficients are corrected in their studies rather than using the consistent unity value.

3.3 Light absorption of BrC

As discussed in Section 2.3.2, the realistic AAE_{BC} value for the BC-containing aerosols, which can be affected significantly by coating materials, core sizes, mixing states, and morphologies (Lack & Langridge, 2013; Li et al., 2019), was used to calculate the BrC light absorption at the short wavelengths. In this study, a simple method that combine the real-time measurements of AMS and Aethalometer is adopted to constrain the realistic AAE_{BC} during the three campaigns (Yuan et al., 2016). Good linear relationships between the AAE and the mass ratio of organic aerosol to BC ($r_{Org/BC}$) within equal intervals were found for each campaign, with correlation coefficients (R^2) between 0.57 and 0.96 (Figure 3). Hence, the fitted intercepts of 1.187, 1.042, and 1.086, where the $r_{Org/BC}$ was equal to zero, were regarded as the calculated realistic AAE_{BC} with no contribution from organic matters during the three campaigns. These AAE_{BC} values were obviously higher than those (0.63−0.89) obtained from both urban campaigns and roadway tunnel experiments in Yuan et al. (2016) where BC were mainly from the fossil fuel combustion, however, comparable or even much lower than those (up to 8.27) for biomass burning emissions, suggesting that the AAE_{BC} might be associated tightly with the BC sources. A higher AAE_{BC} was found at QOMS during the three campaign, consistent with the significant influence from long-range transported biomass burning aerosols at this site. Noting that this is a simple method to estimate the near-realistic AAE_{BC} value, the real AAE_{BC} might be quite complicated and difficult to simulate. Besides, the constant AAE_{BC} derived from the entire period of the campaign might have biased from the real time dependent AAE_{BC}.

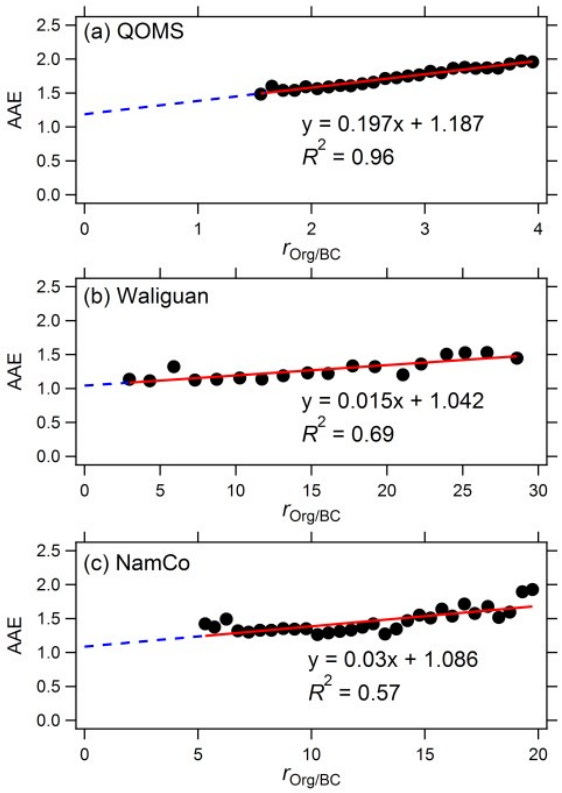

Figure 3. Calculations of AAE_{BC} with the linear relationships between AAE and $r_{Org/BC}$ at the three measurement campaigns. The solid red lines are the linear fitting lines, while the dotted blue lines are the corresponding extended lines to show the obtained AAE_{BC} values at where $r_{Org/BC} = 0$.

The particle light absorption coefficients attributed to BC ($B_{abs,BC}$) and BrC ($B_{abs,BrC}$) at the seven wavelengths during each campaign are show in Figure 4 and Table S1. Both the $B_{abs,BC}$ and $B_{abs,BrC}$ as well as the BrC contribution to total absorption decreased significantly with the increasing wavelength at the three sites. Although BC was the main light-absorbing component that dominated more than 60% of the total B_{abs} among the three campaigns, BrC still showed important contributions at the short wavelengths. The campaign-averaged $B_{abs,BrC}$ at 370 nm ($B_{abs,BrC,370}$) were 4.4, 0.6, and 0.7 Mm^{-1} during the QOMS, Waliguan and NamCo, respectively, which contributed 33.1%, 22.4%, and 21.3% of the total light absorption at 370 nm, correspondingly. Similar as the total light absorption, $B_{abs,BrC,370}$ at NamCo and Waliguan were extremely low due to the low aerosol mass loadings and limited abundance of light-absorbing matters, whereas relatively higher $B_{abs,BrC,370}$ and higher BrC contributions at QOMS might associate with the important contributions of light-absorbing nitrogen-containing compounds from the transported biomass burning emissions (An et al., 2019; Xu et al., 2020). These differences reveal again the remarkably different absorption properties of aerosol over different regions of TP. The average $B_{abs,BrC,370}$ at QOMS was comparable with those at other urban (Lhasa; 4.2 Mm^{-1}) or remote (Lulang; 4.8 Mm^{-1}) sites over the TP (Zhu et al., 2017), but obviously lower than those at relatively polluted urban cities like Beijing, Guangzhou, and Panyu in China during the winter season (Li et al., 2019; Qin et al., 2018; Xie et al., 2019), as listed in Table 1. The campaign-averaged BrC AAE (AAE_{BrC}), also calculated through a power-law fitting of the BrC light absorption coefficients between 370 and 660 nm, were 4.21, 3.11, and 3.71 during the QOMS, Waliguan and NamCo campaigns, respectively. The situation of higher BrC AAE at

QOMS but lower value at Waliguan was quite consistent with those results of AAE values from water-soluble BrC (WS-BrC) among the three campaigns, e.g., 6.83 for QOMS versus 5.96 for Waliguan and 6.19 for NamCo (Xu et al., 2020; Zhang et al., 2017).

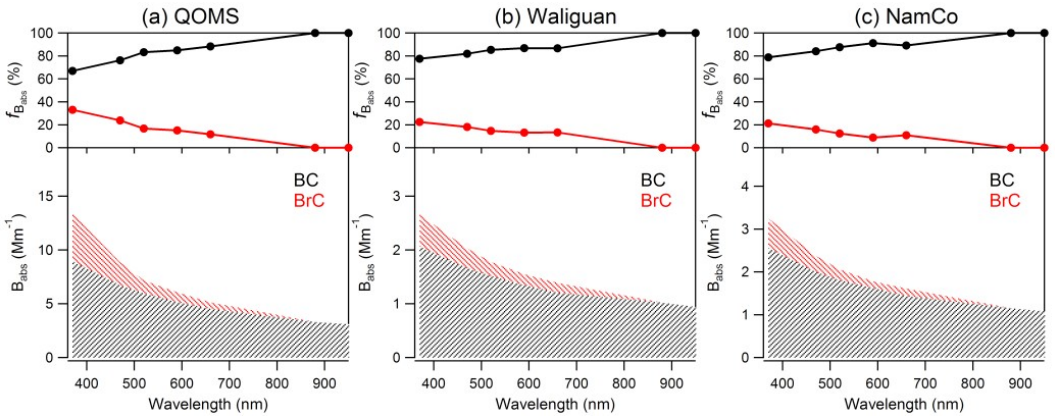

Figure 4. Contributions of BC and BrC to the total particle light absorption coefficient at different wavelengths at the three measurement campaigns.

3.4 The sources of BrC based on light absorption apportionment

The sources of BrC are explored by the linear decomposition of the light absorption of BrC to different OA components apportioned from the HR-ToF-AMS measurement in this study. Since the extremely low BrC light absorption and low signal-to-noise ratios at Waliguan and Namco, this analysis is only performed on the dataset of QOMS. Source apportionment of OA via positive matrix factorization (PMF) analysis identified three distinct OA factors during the QOMS campaign, including a biomass burning related OA (BBOA), a nitrogen-containing OA (NOA) and a more-oxidized oxygenated OA (MO-OOA), with the average mass concentrations of 1.05, 0.34, and 1.02 μg m^{-3}, respectively (Zhang et al., 2018). The temporal variations and scatter plots of $B_{abs,BrC,370}$ and mass concentrations of the three OA components are display in Figure S5. The $B_{abs,BrC,370}$ correlated well (R^2 = 0.81) with the BBOA mass concentrations, while moderate correlations were found between $B_{abs,BrC,370}$ and the concentrations of MO-OOA and NOA (R^2 = 0.32 and 0.37), suggesting probably dominant contribution from BBOA to the total $B_{abs,BrC,370}$. Specifically, the contributions from different OA components to the total BrC absorptions at 370−660 nm were calculated via the multiple regression analysis, respectively, as described in the following equation (3):

$$B_{abs,BrC,\lambda} = a \times [BBOA] + b \times [MO\text{-}OOA] + c \times [NOA] \quad (3)$$

where $B_{abs,BrC,\lambda}$ is the total BrC absorption coefficients (Mm^{-1}) at a certain wavelength λ; [BBOA], [MO-OOA], and [NOA] are the mass concentrations of each OA component (μg m^{-3}); a, b, and c are the fitted regression coefficients (m^2 g^{-1}), which also represent the MAC value for each OA component. Hence, each item, e.g., a × [BBOA], can be calculated as the apportioned light absorption from the certain OA component.

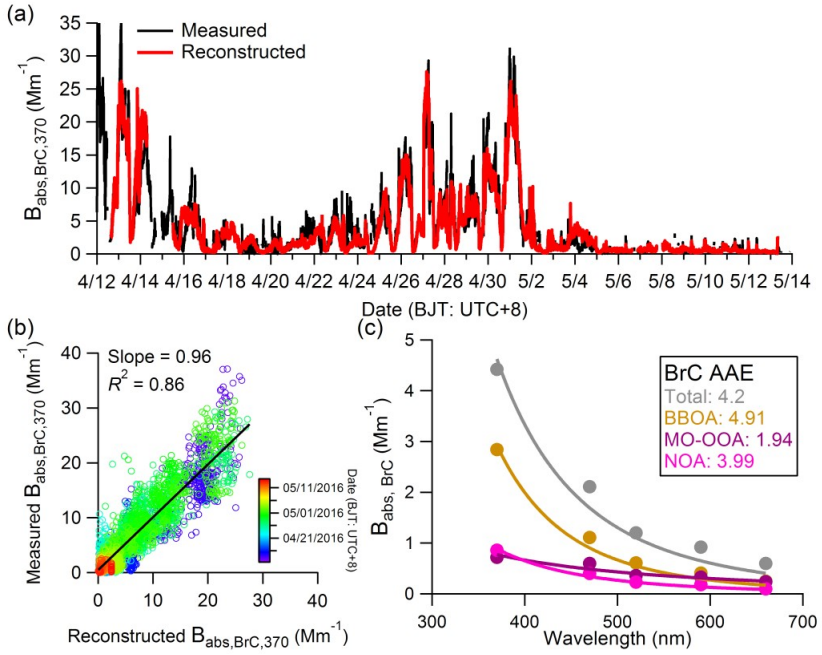

Figure 5. Apportionments of the BrC light absorption coefficient ($B_{abs,BrC}$) to different light-absorbing organic components using the multiple regression analysis at QOMS campaign. **(a)** Time series and **(b)** scatter plot of the measured and reconstructed $B_{abs,BrC}$ at 370 nm ($B_{abs,BrC,370}$) during the sampling period, and **(c)** the average $B_{abs,BrC}$ absorbed by different light-absorbing organic components at wavelengths between 370 nm and 660 nm.

The comparisons between the calculated $B_{abs,BrC}$ and the reconstructed $B_{abs,BrC}$ at 370 nm are shown in Figure 5. Quite perfect reconstruction with slope near to 1 and high correlation coefficient of 0.86 was derived, suggesting the well performance using the multiple regression analysis method to apportion the total $B_{abs,BrC}$ to different BrC sources in this study. The fitted MAC values at 370 nm were 2.29, 2.18, and 0.60 m^2 g^{-1} for BBOA, NOA, and MO-OOA, respectively (Table 2). The relatively high MAC values for the relatively fresh BBOA and NOA were consistent with the findings in those previous studies that nitrogen-containing organics, especially CHON compounds, contributed substantially to the particle light absorption (An et al., 2019; Chen et al., 2016; Xu et al., 2020). Whereas low MAC of MO-OOA suggested that the photolysis and/or photochemistry oxidation processes could cause significant photo-bleaching of BrC chromophores and hence decrease the BrC absorptivity (Chen et al., 2020; Sareen et al., 2013; Wong et al., 2017). In addition, the MAC values for each OA component decreased obviously with the increased wavelengths from 370 nm to 660 nm, however, the differences among the three OA components weakened at the longer wavelengths, e.g., almost identical MAC values at 660 nm, which were mainly associated with the different wave-dependency properties (e.g., different AAE values) for different OA components. Specifically, BBOA contributed for 64.2% of the total $B_{abs,BrC}$ at 370 nm, while deceased to 42.3% at 660 nm with a fitted higher AAE value of 4.91, whereas the MO-OOA contributions increased correspondingly from 16.3% to 41.0% and characterized by a lower AAE value of 1.94. NOA, which contributed just 13.9% of the total OA mass concentration, showed a nearly stable contributions (16.7−19.5%) to total BrC absorptions among all wavelengths during the QOMS campaign.

Table 2. The mass absorption cross-section (MAC) values and the fractions (*f*) of light absorption coefficient for different organic components resolved by the AMS/PMF measurements to total BrC light absorption coefficient at different wavelengths (370-660 nm) during the QOMS campaign.

	370 nm		470 nm		520 nm		590 nm		660 nm	
	MAC (m^2 g^{-1})	*f* (%)	MAC (m^2 g^{-1})	*f* (%)	MAC (m^2 g^{-1})	*f* (%)	MAC (m^2 g^{-1})	*f* (%)	MAC (m^2 g^{-1})	*f* (%)
BBOA	2.29	64.2	0.92	52.7	0.51	51.1	0.35	44.9	0.21	42.3
MO-OOA	0.60	16.3	0.51	28.3	0.31	30.1	0.29	36.0	0.21	41.0
NOA	2.18	19.5	1.04	19.0	0.59	18.8	0.47	19.2	0.26	16.7

3.5 Impacts on radiative forcing

The performance of OPAC model need to be firstly evaluated and tuned before the simulation of DRF in SBDART model by comparing those modelled and measured light scattering and absorption coefficients. The comparisons between modelled light scattering and absorption coefficients from OPAC model and those correspondingly measured values from online Aethalometer and PAX measurements during the three campaigns were shown in Figure S6 in this study. Consistent variation trends were found with correlation coefficients varied between 0.69 and 0.99. The slightly lower modelled values compared with those measured values mainly attributed to their inconsistent wavelengths, e.g., modelled light scattering and absorption coefficients at 550 nm in the OPAC model whereas measured light scattering coefficients at 405 nm for PAX and light absorption coefficients at 520 nm for Aethalometer. Overall, small differences between the modelled and measured values generally indicated the reasonable simulations of aerosol optical parameters (e.g., AOD, AE, SSA, and ASY) in the OPAC model in this study.

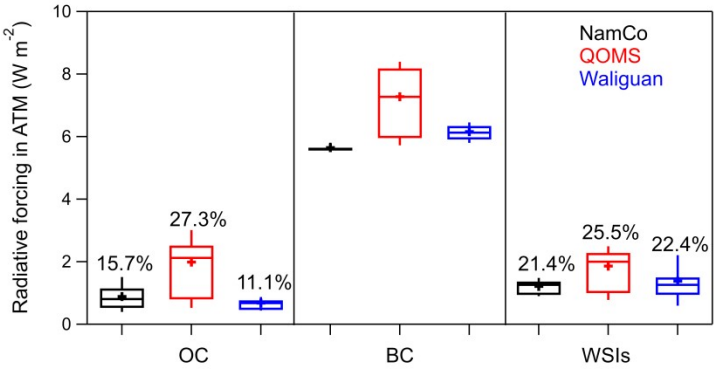

Figure 6. Box-plots of the modelled direct radiative forcing (DRF) in the atmosphere (ATM) caused by organic carbon (OC), black carbon (BC), and water soluble ions (WSIs) during the three campaigns. The whiskers indicate the 90th and 10th percentiles, the upper and lower boundaries of boxes indicate the 75th and 25th percentiles, the lines in the boxes indicate the median values, and the markers indicate the mean values. The percentage values represented the ratios of DRFs from OC and WSIs to those from BC, respectively.

Box-plots of the modelled atmospheric DRFs caused by OC, BC, and WSIs during the three campaigns were shown in Figure 6. Actually, BC produced remarkable warm effects at the TOA with average DRF values of +2.5 ± 0.5, +2.1 ± 0.1, and +1.9 ± 0.1 W m^{-2} during the

441 QOMS, Waliguan and NamCo campaigns, respectively. In contrast, obviously cooling effects
442 caused by BC were found at the SUR with average DRFs of −4.7 ± 0.8, −4.1 ± 0.2, and −3.7 ±
443 0.1 W m^{-2} among the three campaigns. The warm effect at the TOA but cooling effect at the
444 SUR induced by BC finally resulted significantly high net atmospheric forcings of +7.3 ± 1.2,
445 +6.2 ± 0.3, and +5.6 ± 0.2 W m^{-2} during the QOMS, Waliguan and NamCo campaigns,
446 respectively, suggesting the important radiative effect caused by BC in the TP, especially in the
447 southern TP regions where has been revealed to be significantly influenced by the long-range
448 transported biomass burning emissions from South Asia. Comparatively, negative and low
449 average DRFs were found at the TOA and SUR for both OC and WSIs and finally generated
450 much lower net atmospheric forcings among the three campaigns compared with those for BC,
451 e.g., +2.0 ± 1.2, +0.7 ± 0.2, and +0.9 ± 0.7 W m^{-2} for OC and +1.9 ± 0.8, +1.4 ± 0.6, and +1.2 ±
452 0.2 W m^{-2} for WSIs at QOMS, Waliguan and NamCo, respectively. Interestingly, the average
453 atmospheric DRF of OC could reached 27.3% of that of BC at QOMS whereas only 11.1% and
454 15.7% at Waliguan and NamCo. The highest net atmospheric DRFs of BC and OC at QOMS
455 among the three campaigns mainly associated with the distinctly different chemical compositions
456 and light absorption properties of aerosols in the different TP regions. The dominant
457 contributions of carbonaceous aerosols especially those light-absorbing BC and BrC aerosols at
458 QOMS in the southern TP might induce obviously higher atmospheric DRFs than those at
459 Waliguan and NamCo in the northern and central TP.

460 **4 Conclusions**

461 This study explored the regional differences of chemical compositions and light
462 absorption properties of aerosols at three high-altitude remote sites (QOMS, NamCo, and
463 Waliguan) over the Tibetan Plateau. Relatively lower PM_1 mass concentrations (4.4 and 2.0 μg
464 m^{-3}) with dominant contributions from organics and BC were observed at QOMS in the southern
465 TP and NamCo in the central TP, whereas higher PM_1 mass concentration (9.1 μg m^{-3}) and
466 higher contributions of secondary inorganic species were observed at Waliguan in the northern
467 TP. This difference on aerosol chemical speciation may be attributed to the differences in aerosol
468 sources in the regions around them. Although lower aerosol mass loading was found at QOMS,
469 the campaign-averaged light absorption coefficient (13.4 Mm^{-1}) at QOMS in the southern TP
470 was much higher than that (2.7 Mm^{-1}) measured at Waliguan in the northern TP, suggesting the
471 dominant contributions of light-absorbing carbonaceous aerosols (both BC and BrC) from
472 biomass burning emissions in the southern TP. Correspondingly, the AAE values are fitted to be
473 1.73, 1.12 and 1.28 at QOMS, Waliguan and NamCo, respectively. The higher AAE at QOMS
474 suggested its higher contribution of BrC. In order to obtain the BrC light absorption at the short
475 wavelengths, an improved method was adopted in this study to derive the near realistic AAE
476 value for pure BC particle (AAE_{BC}) during the three campaigns. The AAE_{BC} values were
477 calculated as 1.187, 1.042, and 1.086 during the three campaigns by exploring the linear
478 relationships between AAE and mass ratio of organic aerosol to BC, respectively. Although BC
479 was the main light-absorbing component, BrC still showed important contributions to the total
480 B_{abs} at the short wavelengths during the three campaigns. BrC could contribute more than 30% of
481 the total light absorption coefficient at 370 nm during the QOMS campaign whereas only 20% at
482 Waliguan and NamCo. The sources of BrC at QOMS were further explored through the linear
483 decomposition of BrC light absorption to different OA components apportioned from the HR-
484 ToF-AMS measurement. BBOA contributed 64.2% of the total BrC light absorption at 370 nm,
485 however, the contributions decreased significantly with the increasing wavelength following a

high BrC AAE value of 4.91. On the contrary, the contributions of MO-OOA increased from 16.3% to 41.0% with the increasing wavelength while NOA showed a nearly stable contributions (16.7−19.5%) among all wavelengths. The MAC values for BBOA and NOA (2.29 and 2.18 m^2 g^{-1}) were much higher than that (0.60 m^2 g^{-1}) for the MO-OOA, consistent with the previous findings that nitrogen-containing organics contributed substantially to the particle light absorption. The radiative transfer model showed that the net atmospheric forcings caused by BC were +7.3 ± 1.2, +6.2 ± 0.3, and +5.6 ± 0.2 W m^{-2} during the QOMS, Waliguan and NamCo campaigns, respectively, while the atmospheric DRFs of OC could reached 27.3%, 11.1%, and 15.7% to those of BC, suggesting the important radiative effect caused by carbonaceous aerosols in the TP, especially in the southern TP regions. Overall, the regional difference on the chemical compositions and light absorption properties of aerosols over the different TP regions need be take into account in the climate models for the evaluation of radiant energy budget as well as the potential impacts on climate and cryospheric change over the Third Pole environments.

Acknowledgments and Data Access

This research was supported by the National Natural Science Foundation of China (41977189, 41771079, 41605119, and 41805106), the second Tibetan Plateau Scientific Expedition and Research Program (STEP) (2019QZKK0605), the Key Laboratory of Cryospheric Sciences Scientific Research Foundation (SKLCS-ZZ-2020). The authors show great thanks to the Nam Co Station for Multisphere Observation and Research, Chinese Academy of Sciences, the Qomolangma Station for Atmospheric and Environmental Observation and Research, Chinese Academy of Sciences, and the Waliguan Baseline Observatory for their logistical supports. The data in this manuscript are available at https://www.zenodo.org/deposit/3987000#.

References

An, Y., Xu, J., Feng, L., Zhang, X., Liu, Y., Kang, S., et al. (2019). Molecular characterization of organic aerosol in the Himalayas: insight from ultra-high-resolution mass spectrometry. *Atmospheric Chemistry and Physics*, *19*(2), 1115-1128. https://doi.org/10.5194/acp-19-1115-2019

Andreae, M. O. & Gelencsér, A. (2006). Black carbon or brown carbon? The nature of light-absorbing carbonaceous aerosols. *Atmospheric Chemistry and Physics*, *6*(10), 3131-3148. https://doi.org/10.5194/acp-6-3131-2006

Bond, T. C., Doherty, S. J., Fahey, D. W., Forster, P. M., Berntsen, T., DeAngelo, B. J., et al. (2013). Bounding the role of black carbon in the climate system: A scientific assessment. *Journal of Geophysical Research: Atmospheres*, *118*(11), 5380-5552. https://doi.org/10.1002/jgrd.50171

Cao, J., Tie, X., Xu, B., Zhao, Z., Zhu, C., Li, G., et al. (2011). Measuring and modeling black carbon (BC) contamination in the SE Tibetan Plateau. *Journal of Atmospheric Chemistry*, *67*(1), 45-60. https://doi.org/10.1007/s10874-011-9202-5

Chen, Q., Ikemori, F. & Mochida, M. (2016). Light Absorption and Excitation-Emission Fluorescence of Urban Organic Aerosol Components and Their Relationship to Chemical Structure. *Environmental Science & Technology*, *50*(20), 10859-10868. https://doi.org/10.1021/acs.est.6b02541

Chen, X., Kang, S., Cong, Z., Yang, J. & Ma, Y. (2018a). Concentration, temporal variation, and sources of black carbon in the Mt. Everest region retrieved by real-time observation and

simulation. *Atmospheric Chemistry and Physics*, *18*(17), 12859-12875. https://doi.org/10.5194/acp-18-12859-2018

Chen, Y., Ge, X., Chen, H., Xie, X., Chen, Y., Wang, J., et al. (2018b). Seasonal light absorption properties of water-soluble brown carbon in atmospheric fine particles in Nanjing, China. *Atmospheric Environment*, *187*, 230-240. https://doi.org/10.1016/j.atmosenv.2018.06.002

Chen, Y., Xie, X., Shi, Z., Li, Y., Gai, X., Wang, J., et al. (2020). Brown carbon in atmospheric fine particles in Yangzhou, China: Light absorption properties and source apportionment. *Atmospheric Research*, *244*, 105028. https://doi.org/10.1016/j.atmosres.2020.105028

Collaud Coen, M., Weingartner, E., Apituley, A., Ceburnis, D., Fierz-Schmidhauser, R., Flentje, H., et al. (2010). Minimizing light absorption measurement artifacts of the Aethalometer: evaluation of five correction algorithms. *Atmospheric Measurement Techniques*, *3*(2), 457-474. https://doi.org/10.5194/amt-3-457-2010

Cong, Z., Kang, S., Kawamura, K., Liu, B., Wan, X., Wang, Z., et al. (2015a). Carbonaceous aerosols on the south edge of the Tibetan Plateau: concentrations, seasonality and sources. *Atmospheric Chemistry and Physics*, *15*(3), 1573-1584. https://doi.org/10.5194/acp-15-1573-2015

Cong, Z., Kawamura, K., Kang, S. & Fu, P. (2015b). Penetration of biomass-burning emissions from South Asia through the Himalayas: new insights from atmospheric organic acids. *Scientific reports*, *5*, 9580. https://doi.org/10.1038/srep09580

Corr, C. A., Hall, S. R., Ullmann, K., Anderson, B. E., Beyersdorf, A. J., Thornhill, K. L., et al. (2012). Spectral absorption of biomass burning aerosol determined from retrieved single scattering albedo during ARCTAS. *Atmospheric Chemistry and Physics*, *12*(21), 10505-10518. https://doi.org/10.5194/acp-12-10505-2012

Drinovec, L., Močnik, G., Zotter, P., Prévôt, A. S. H., Ruckstuhl, C., Coz, E., et al. (2015). The "dual-spot" Aethalometer: an improved measurement of aerosol black carbon with real-time loading compensation. *Atmospheric Measurement Techniques*, *8*(5), 1965-1979. https://doi.org/10.5194/amt-8-1965-2015

Duan, A. M. & Wu, G. X. (2005). Role of the Tibetan Plateau thermal forcing in the summer climate patterns over subtropical Asia. *Climate Dynamics*, *24*(7-8), 793-807. https://doi.org/10.1007/s00382-004-0488-8

Favez, O., Alfaro, S. C., Sciare, J., Cachier, H. & Abdelwahab, M. M. (2009). Ambient measurements of light-absorption by agricultural waste burning organic aerosols. *Journal of Aerosol Science*, *40*(7), 613-620. https://doi.org/10.1016/j.jaerosci.2009.04.002

Feng, Y., Ramanathan, V. & Kotamarthi, V. R. (2013). Brown carbon: a significant atmospheric absorber of solar radiation? *Atmospheric Chemistry and Physics*, *13*(17), 8607-8621. https://doi.org/10.5194/acp-13-8607-2013

Gong, C., Xin, J., Wang, S., Wang, Y. & Zhang, T. (2017). Anthropogenic aerosol optical and radiative properties in the typical urban/suburban regions in China. *Atmospheric Research*, *197*, 177-187. https://doi.org/10.1016/j.atmosres.2017.07.002

Gyawali, M., Arnott, W. P., Lewis, K. & Moosmüller, H. (2009). In situ aerosol optics in Reno, NV, USA during and after the summer 2008 California wildfires and the influence of absorbing and non-absorbing organic coatings on spectral light absorption. *Atmospheric Chemistry and Physics*, *9*(20), 8007-8015. https://doi.org/10.5194/acp-9-8007-2009

Hess, M., Koepke, P. & Schult, I. (1998). Optical Properties of Aerosols and Clouds: The Software Package OPAC. *Bulletin of the American Meteorological Society*, *79*, 831-844. https://doi.org/10.1175/1520-0477(1998)079<0831:OPOAAC>2.0.CO;2

Jacobson, M. Z. (2001). Strong radiative heating due to the mixing state of black carbon in atmospheric aerosols. *Nature*, *409*(6821), 695-697. https://doi.org/10.1038/35055518

Kang, S., Xu, Y., You, Q., Flügel, W.-A., Pepin, N. & Yao, T. (2010). Review of climate and cryospheric change in the Tibetan Plateau. *Environmental Research Letters*, *5*(1), 015101. https://doi.org/10.1088/1748-9326/5/1/015101

Kang, S., Zhang, Q., Qian, Y., Ji, Z., Li, C., Cong, Z., et al. (2019). Linking atmospheric pollution to cryospheric change in the Third Pole region: current progress and future prospects. *National Science Review*, *6*(4), 796-809. https://doi.org/10.1093/nsr/nwz031

Kirillova, E. N., Marinoni, A., Bonasoni, P., Vuillermoz, E., Facchini, M. C., Fuzzi, S., et al. (2016). Light absorption properties of brown carbon in the high Himalayas. *Journal of Geophysical Research: Atmospheres*, *121*(16), 9621-9639. https://doi.org/10.1002/2016jd025030

Lack, D. A. & Cappa, C. D. (2010). Impact of brown and clear carbon on light absorption enhancement, single scatter albedo and absorption wavelength dependence of black carbon. *Atmospheric Chemistry and Physics*, *10*(9), 4207-4220. https://doi.org/10.5194/acp-10-4207-2010

Lack, D. A. & Langridge, J. M. (2013). On the attribution of black and brown carbon light absorption using the Ångström exponent. *Atmospheric Chemistry and Physics*, *13*(20), 10535-10543. https://doi.org/10.5194/acp-13-10535-2013

Laskin, A., Laskin, J. & Nizkorodov, S. A. (2015). Chemistry of atmospheric brown carbon. *Chemical reviews*, *115*(10), 4335-4382. https://doi.org/10.1021/cr5006167

Lewis, K., Arnott, W. P., Moosmüller, H. & Wold, C. E. (2008). Strong spectral variation of biomass smoke light absorption and single scattering albedo observed with a novel dual-wavelength photoacoustic instrument. *Journal of Geophysical Research: Atmospheres*, *113*(D16), D16203.

Li, C., Bosch, C., Kang, S., Andersson, A., Chen, P., Zhang, Q., et al. (2016a). Sources of black carbon to the Himalayan-Tibetan Plateau glaciers. *Nature communications*, *7*, 12574. https://doi.org/10.1038/ncomms12574

Li, C., Yan, F., Kang, S., Chen, P., Hu, Z., Gao, S., et al. (2016b). Light absorption characteristics of carbonaceous aerosols in two remote stations of the southern fringe of the Tibetan Plateau, China. *Atmospheric Environment*, *143*, 79-85. https://doi.org/10.1016/j.atmosenv.2016.08.042

Li, W. J., Chen, S. R., Xu, Y. S., Guo, X. C., Sun, Y. L., Yang, X. Y., et al. (2015). Mixing state and sources of submicron regional background aerosols in the northern Qinghai–Tibet Plateau and the influence of biomass burning. *Atmospheric Chemistry and Physics*, *15*(23), 13365-13376. https://doi.org/10.5194/acp-15-13365-2015

Li, Z., Tan, H., Zheng, J., Liu, L., Qin, Y., Wang, N., et al. (2019). Light absorption properties and potential sources of particulate brown carbon in the Pearl River Delta region of China. *Atmospheric Chemistry and Physics*, *19*(18), 11669-11685. https://doi.org/10.5194/acp-19-11669-2019

Lin, P., Aiona, P. K., Li, Y., Shiraiwa, M., Laskin, J., Nizkorodov, S. A., et al. (2016). Molecular Characterization of Brown Carbon in Biomass Burning Aerosol Particles. *Environmental Science & Technology*, *50*(21), 11815-11824. https://doi.org/10.1021/acs.est.6b03024

Lu, J., Ge, X., Liu, Y., Chen, Y., Xie, X., Ou, Y., et al. (2019). Significant secondary organic aerosol production from aqueous-phase processing of two intermediate volatility organic

620 compounds. *Atmospheric Environment*, *211*, 63-68.
621 https://doi.org/10.1016/j.atmosenv.2019.05.014
622 Lüthi, Z. L., Škerlak, B., Kim, S. W., Lauer, A., Mues, A., Rupakheti, M., et al. (2015).
623 Atmospheric brown clouds reach the Tibetan Plateau by crossing the Himalayas. *Atmospheric*
624 *Chemistry and Physics*, *15*(11), 6007-6021. https://doi.org/10.5194/acp-15-6007-2015
625 Moosmüller, H., Chakrabarty, R. K., Ehlers, K. M. & Arnott, W. P. (2011). Absorption
626 Ångström coefficient, brown carbon, and aerosols: basic concepts, bulk matter, and spherical
627 particles. *Atmospheric Chemistry and Physics*, *11*(3), 1217-1225. https://doi.org/10.5194/acp-
628 11-1217-2011
629 Qin, J., Yang, K., Liang, S. & Guo, X. (2009). The altitudinal dependence of recent rapid
630 warming over the Tibetan Plateau. *Climatic Change*, *97*(1-2), 321-327.
631 https://doi.org/10.1007/s10584-009-9733-9
632 Qin, Y. M., Tan, H. B., Li, Y. J., Li, Z. J., Schurman, M. I., Liu, L., et al. (2018). Chemical
633 characteristics of brown carbon in atmospheric particles at a suburban site near Guangzhou,
634 China. *Atmospheric Chemistry and Physics*, *18*(22), 16409-16418.
635 https://doi.org/10.5194/acp-18-16409-2018
636 Ramanathan, V. & Carmichael, G. (2008). Global and regional climate changes due to black
637 carbon. *Nature Geoscience*, *1*(4), 221-227. https://doi.org/10.1038/ngeo156
638 Ricchiazzi, P., Yang, S., Gautier, C. & Sowle, D. (1998). SBDART: A Research and Teaching
639 Software Tool for Plane-Parallel Radiative Transfer in the Earth's Atmosphere. *Bulletin of the*
640 *American Meteorological Society*, *79*(10), 2101-2114. https://doi.org/10.1175/1520-
641 0477(1998)079<2101:Sarats>2.0.Co;2
642 Sareen, N., Moussa, S. G. & Mcneill, V. F. (2013). Photochemical Aging of Light-Absorbing
643 Secondary Organic Aerosol Material. *Journal of Physical Chemistry A*, *117*(14), 2987-2996.
644 https://doi.org/10.1021/jp309413j
645 Sun, H., Biedermann, L. & Bond, T. C. (2007). Color of brown carbon: A model for ultraviolet
646 and visible light absorption by organic carbon aerosol. *Geophysical Research Letters*, *34*(17),
647 L17813.
648 Wang, B., Bao, Q., Hoskins, B., Wu, G. & Liu, Y. (2008). Tibetan Plateau warming and
649 precipitation changes in East Asia. *Geophysical Research Letters*, *35*(14),
650 https://doi.org/10.1029/2008gl034330
651 Wang, J., Nie, W., Cheng, Y., Shen, Y., Chi, X., Wang, J., et al. (2018). Light absorption of
652 brown carbon in eastern China based on 3-year multi-wavelength aerosol optical property
653 observations and an improved absorption Ångström exponent segregation method.
654 *Atmospheric Chemistry and Physics*, *18*(12), 9061-9074. https://doi.org/10.5194/acp-18-9061-
655 2018
656 Wang, J., Zhang, Q., Chen, M., Collier, S., Zhou, S., Ge, X., et al. (2017). First Chemical
657 Characterization of Refractory Black Carbon Aerosols and Associated Coatings over the
658 Tibetan Plateau (4730 m a.s.l). *Environmental Science & Technology*, *51*(24), 14072-14082.
659 https://doi.org/10.1021/acs.est.7b03973
660 Wang, Q., Han, Y., Ye, J., Liu, S., Pongpiachan, S., Zhang, N., et al. (2019a). High Contribution
661 of Secondary Brown Carbon to Aerosol Light Absorption in the Southeastern Margin of
662 Tibetan Plateau. *Geophysical Research Letters*, *46*(9), 4962-4970.
663 https://doi.org/10.1029/2019gl082731
664 Wang, Q., Ye, J., Wang, Y., Zhang, T., Ran, W., Wu, Y., et al. (2019b). Wintertime Optical
665 Properties of Primary and Secondary Brown Carbon at a Regional Site in the North China

Plain. *Environmental Science & Technology*, *53*(21), 12389-12397. https://doi.org/10.1021/acs.est.9b03406

Washenfelder, R. A., Attwood, A. R., Brock, C. A., Guo, H., Xu, L., Weber, R. J., et al. (2015). Biomass burning dominates brown carbon absorption in the rural southeastern United States. *Geophysical Research Letters*, *42*(2), 653-664. https://doi.org/10.1002/2014gl062444

Weingartner, E., Saathoff, H., Schnaiter, M., Streit, N., Bitnar, B. & Baltensperger, U. (2003). Absorption of light by soot particles: determination of the absorption coefficient by means of aethalometers. *Journal of Aerosol Science*, *34*(10), 1445-1463. https://doi.org/10.1016/s0021-8502(03)00359-8

Wong, J. P. S., Nenes, A. & Weber, R. J. (2017). Changes in Light Absorptivity of Molecular Weight Separated Brown Carbon Due to Photolytic Aging. *Environmental Science & Technology*, *51*(15), 8414-8421. https://doi.org/10.1021/acs.est.7b01739

Wu, C., Wu, D. & Yu, J. Z. (2018). Quantifying black carbon light absorption enhancement with a novel statistical approach. *Atmospheric Chemistry and Physics*, *18*(1), 289-309. https://doi.org/10.5194/acp-18-289-2018

Wu, G., Wan, X., Ram, K., Li, P., Liu, B., Yin, Y., et al. (2020). Light absorption, fluorescence properties and sources of brown carbon aerosols in the Southeast Tibetan Plateau. *Environmental Pollution*, *257*, 113616. https://doi.org/10.1016/j.envpol.2019.113616

Xie, C., Xu, W., Wang, J., Wang, Q., Liu, D., Tang, G., et al. (2019). Vertical characterization of aerosol optical properties and brown carbon in winter in urban Beijing, China. *Atmospheric Chemistry and Physics*, *19*(1), 165-179. https://doi.org/10.5194/acp-19-165-2019

Xin, J., Gong, C., Wang, S. & Wang, Y. (2016). Aerosol direct radiative forcing in desert and semi-desert regions of northwestern China. *Atmospheric Research*, *171*, 56-65. https://doi.org/10.1016/j.atmosres.2015.12.004

Xu, B., Cao, J., Hansen, J., Yao, T., Joswia, D. R., Wang, N., et al. (2009). Black soot and the survival of Tibetan glaciers. *Proceedings of the National Academy of Sciences of the United States of America*, *106*(52), 22114-22118. https://doi.org/10.1073/pnas.0910444106

Xu, J., Hettiyadura, A. P. S., Liu, Y., Zhang, X., Kang, S. & Laskin, A. (2020). Regional Differences of Chemical Composition and Optical Properties of Aerosols in the Tibetan Plateau. *Journal of Geophysical Research: Atmospheres*, *125*(1), https://doi.org/10.1029/2019jd031226

Xu, J., Wang, Z., Yu, G., Qin, X., Ren, J. & Qin, D. (2014). Characteristics of water soluble ionic species in fine particles from a high altitude site on the northern boundary of Tibetan Plateau: Mixture of mineral dust and anthropogenic aerosol. *Atmospheric Research*, *143*, 43-56. https://doi.org/http://dx.doi.org/10.1016/j.atmosres.2014.01.018

Xu, J., Zhang, Q., Shi, J., Ge, X., Xie, C., Wang, J., et al. (2018). Chemical characteristics of submicron particles at the central Tibetan Plateau: insights from aerosol mass spectrometry. *Atmospheric Chemistry and Physics*, *18*(1), 427-443. https://doi.org/10.5194/acp-18-427-2018

Yan, C., Zheng, M., Bosch, C., Andersson, A., Desyaterik, Y., Sullivan, A. P., et al. (2017). Important fossil source contribution to brown carbon in Beijing during winter. *Scientific reports*, *7*, 43182. https://doi.org/10.1038/srep43182

Yao, T., Thompson, L., Mosbrugger, V., Zhang, F., Ma, Y., Luo, T., et al. (2012). Third Pole Environment (TPE). *Environmental Development*, *3*, 52-64. https://doi.org/10.1016/j.envdev.2012.04.002

Ye, Z., Qu, Z., Ma, S., Luo, S., Chen, Y., Chen, H., et al. (2019). A comprehensive investigation of aqueous-phase photochemical oxidation of 4-ethylphenol. *Science of the Total Environment*, *685*, 976-985. https://doi.org/10.1016/j.scitotenv.2019.06.276

Yuan, J. F., Huang, X. F., Cao, L. M., Cui, J., Zhu, Q., Huang, C. N., et al. (2016). Light absorption of brown carbon aerosol in the PRD region of China. *Atmospheric Chemistry and Physics*, *16*(3), 1433-1443. https://doi.org/10.5194/acp-16-1433-2016

Zhang, N., Cao, J., Liu, S., Zhao, Z., Xu, H. & Xiao, S. (2014). Chemical composition and sources of $PM_{2.5}$ and TSP collected at Qinghai Lake during summertime. *Atmospheric Research*, *138*, 213-222. https://doi.org/10.1016/j.atmosres.2013.11.016

Zhang, X., Xu, J., Kang, S., Liu, Y. & Zhang, Q. (2018). Chemical characterization of long-range transport biomass burning emissions to the Himalayas: insights from high-resolution aerosol mass spectrometry. *Atmospheric Chemistry and Physics*, *18*(7), 4617–4638. https://doi.org/10.5194/acp-18-4617-2018

Zhang, X., Xu, J., Kang, S., Zhang, Q. & Sun, J. (2019). Chemical characterization and sources of submicron aerosols in the northeastern Qinghai–Tibet Plateau: insights from high-resolution mass spectrometry. *Atmospheric Chemistry and Physics*, *19*(11), 7897-7911. https://doi.org/10.5194/acp-19-7897-2019

Zhang, Y., Xu, J., Shi, J., Xie, C., Ge, X., Wang, J., et al. (2017). Light absorption by water-soluble organic carbon in atmospheric fine particles in the central Tibetan Plateau. *Environmental Science and Pollution Research*, *24*(26), 21386-21397. https://doi.org/10.1007/s11356-017-9688-8

Zhao, Z., Cao, J., Chow, J. C., Watson, J. G., Chen, A. L. W., Wang, X., et al. (2019). Multi-wavelength light absorption of black and brown carbon at a high-altitude site on the Southeastern margin of the Tibetan Plateau, China. *Atmospheric Environment*, *212*, 54-64. https://doi.org/10.1016/j.atmosenv.2019.05.035

Zhu, C. S., Cao, J. J., Hu, T. F., Shen, Z. X., Tie, X. X., Huang, H., et al. (2017). Spectral dependence of aerosol light absorption at an urban and a remote site over the Tibetan Plateau. *Science of the Total Environment*, *590-591*, 14-21. https://doi.org/10.1016/j.scitotenv.2017.03.057

Zhu, C. S., Cao, J. J., Huang, R. J., Shen, Z. X., Wang, Q. Y. & Zhang, N. N. (2018). Light absorption properties of brown carbon over the southeastern Tibetan Plateau. *Science of the Total Environment*, *625*, 246-251. https://doi.org/10.1016/j.scitotenv.2017.12.183